Channel Estimation for Ambient Backscatter Communication Systems with Massive-Antenna Reader

Wenjing Zhao, Gongpu Wang, *Member, IEEE*, Saman Atapattu, *Senior Member, IEEE*, Ruisi He, *Senior Member, IEEE*, and Ying-Chang Liang, *Fellow, IEEE*

***Abstract*—Ambient backscatter, an emerging green communication technology, has aroused great interest from both academia and industry. One open problem for ambient backscatter communication (AmBC) systems is channel estimation for a massive-antenna reader. In this paper, we focus on channel estimation problem in AmBC systems with uniform linear array (ULA) at the reader which consists of large number of antennas. We first design a two-step method to jointly estimate channel gains and direction of arrivals (DoAs), and then refine the estimates through angular rotation. Additionally, Cramér-Rao lower bounds (CRLBs) are derived for both the modulus of the channel gain and the DoA estimates. Simulations are then provided to validate the analysis, and to show the efficiency of the proposed approach.**

***Index Terms*—Ambient backscatter, channel estimation, direction of arrivals (DoAs), discrete Fourier transformation (DFT)**

I. Introduction

Aiming to enable easy access and interaction among numerous computing devices such as sensors and Internet of Things (IoT) will play a vital role in the future communication paradigm [1], [2]. Recently, there have been a variety of research directions on IoT. Among them, how sustainable and reliable energy can be supplied to large-scale deployments of IoT devices is an interesting and challenging problem nowadays. Since ambient backscatter leverages environmental radio frequency (RF) signals to enable battery-free devices to communicate with each other, it has high potential to offer a solution for the energy problem in IoT systems [3]. An ambient backscatter communication (AmBC) system typically consists of a RF source, reader and tag. Before modulating its own binary data, the tag first harvests energy from RF signals, which thus exempts the tag from energy constraint. Then, the tag loads bit '1' by reflecting the incident RF signals and bit '0' by absorbing them. By using certain detector, such as maximum-likelihood (ML) detector, the reader demodulates the bit information accordingly [4].

The majority of existing theoretical studies on AmBC, related to signal detection [4], [5] and the references therein, performance analysis [6]–[8] and multiple access scheme [9], assume perfect channel state information (CSI). In reality, precise knowledge of full CSI is not always available, especially with strict energy constrained IoT systems. Other than contributing to signal detection, perfect CSI plays a key role in transceiver design and security improvement [10]–[12].

Traditionally, instantaneous channel coefficients can be obtained through the channel estimation and CSI exchange procedure in every coherence time. However, accurate channel estimation may only be possible with reasonably long enough training signals, which costs significant time and power, especially with strict energy-constrained massive-antenna IoT systems. Since the tag in an AmBC system merely modulates its signals by reflecting the incident signals, it is unable to transmit additional training or pilot signals. Therefore, traditional channel estimation techniques may not be directly applied to AmBC systems. Moreover, while RF signals are usually unknown to the both reader and tag, the inconsistencies of channels at reflective and absorptive states also pose great challenges on channel estimation. Taking these into account, an expectation maximization (EM) based estimator is designed to acquire the modulus values of channels in an AmBC system with a single-antenna reader in [13]. In a multiple-antenna reader circumstance, an approach on the strength of eigenvalue decomposition (EVD) [14] is adopted to retrieve channel parameters. Nevertheless, the complexity of EVD is prohibitive in AmBC systems with massive-antenna [15]–[17] reader, which motivates our work. In this paper, we tackle the channel estimation problem in AmBC systems with massive-antenna reader having an uniform linear array (ULA). Together with least-square (LS) method, an estimator resorting to discrete Fourier transformation (DFT) [18] and angular rotation operation is presented to collectively figure out the direction of arrivals (DoAs) and channel gains. To the best of our knowledge, this is the first work which considers on channel estimation for an AmBC system with massive antennas.

Notations: We use boldfaced lowercase for vectors and boldface uppercase for matrices. The transpose and the inverse of matrix $\mathbf{X}$ are denoted by $\mathbf{X}^T$ and $\mathbf{X}^{-1}$, respectively. $[\mathbf{X}]_{ij}$ indicates the (i,j)th element of matrix $\mathbf{X}$, and $\mathbf{x}_i$ indicates the ith element of vector $\mathbf{x}$. $\text{diag}\{\mathbf{x}\}$ denotes a square diagonal matrix with the elements of $\mathbf{x}$ on the main diagonal. The identity matrix is denoted by $\mathbf{I}$. $\mathbf{x} \sim \mathcal{CN}(\boldsymbol{\mu}, \boldsymbol{\Sigma})$ denotes that $\mathbf{x}$ is a circularly symmetric complex Gaussian (CSCG) vector with mean $\boldsymbol{\mu}$ and covariance matrix $\boldsymbol{\Sigma}$. $\|\mathbf{x}\|$ represents the $2-$norm of vector $\mathbf{x}$. $\lfloor x \rceil$ rounds x to the nearest integer, and $\mathbb{E}\{x\}$ means the statistical expectation of x. $\mathfrak{Re}\{x\}$ and $\mathfrak{Im}\{x\}$ denote the real part and the imaginary part of x, respectively.

This work is supported in part by the Fundamental Research Funds for the Central Universities under Grant 2018YJS047 and Grant 2016JBZ006, and in part by the Australian Research Council (ARC) through the Discovery Early Career Researcher (DECRA) Award DE160100020.

W. Zhao and G. Wang are with Beijing Key Lab of Transportation Data Analysis and Mining, School of Computer and Information Technology, Beijing Jiaotong University, China (e-mail: {wenjingzhao, gpwang}@bjtu.edu.cn).

S. Atapattu is with the Department of Electrical and Electronic Engineering, University of Melbourne, Parkville, VIC 3010, Australia (e-mail: saman.atapattu@unimelb.edu.au).

R. He is with the State Key Laboratory of Rail Traffic Control and Safety, Beijing Jiaotong University, China (e-mail: ruisi.he@bjtu.edu.cn).

Y.-C. Liang is with the Center for Intelligent Networking and Communications, University of Electronic Science and Technology of China, Chengdu 611731, China (e-mail: liangyc@ieee.org).

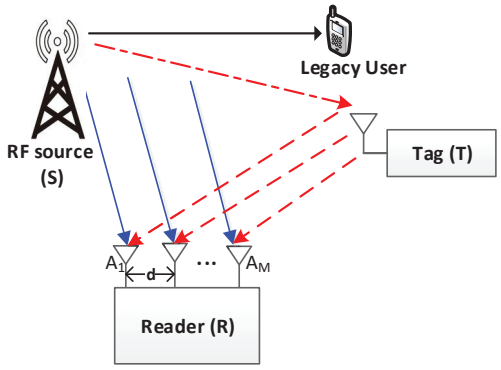

Fig. 1. An ambient backscatter communication (AmBC) system with a massive-antenna reader.

II. System Model

As shown in Fig. 1, we consider an AmBC system with a RF source (S), a reader (R) equipped with M antennas in the form of ULA, and a passive tag (T) with single antenna. The reader not only receives signal from the RF source directly, but also collects signal backscattered from the tag. The tag first harvests energy from the RF signals. By intentionally changing its load impedance, the tag then piggybacks its information bits over ambient RF carriers to backscatter outside or to absorb inside the received signals.

Let $s(n)$ be the signals from the RF source with power P_s and $B(n) \in \{0,1\}$ the modulated signal at the tag which keeps unchanged during N consecutive RF signals. Define $\theta_0 \in [-\frac{\pi}{2}, \frac{\pi}{2}]$ and $\theta_1 \in [-\frac{\pi}{2}, \frac{\pi}{2}]$ as the signal azimuth angles or DoAs of paths $S-R$ and $T-R$, respectively. Denote channel gains of $S-R$, $S-T$ and $T-R$ as h_{sr}, h_{st} and h_{tr}, respectively.[1] The attenuation factor inside the tag is denoted as $\eta \in (0,1]$. Then, the received signal at the reader is [19]

$$\begin{aligned}\mathbf{y}(n) &= \mathbf{h}_{sr}s(n) + \mathbf{h}_{tr}\eta h_{st}s(n)B(n) + \mathbf{w}(n)\\ &= \mathbf{h}s(n) + \mathbf{w}(n),\end{aligned} \tag{1}$$

where the equivalent AmBC channel is

$$\mathbf{h} = \mathbf{h}_{sr} + \eta h_{st}\mathbf{h}_{tr}B(n),$$

$\mathbf{h}_{sr} = h_{sr}[1, e^{j\frac{2\pi d}{\lambda}\sin\theta_0}, \cdots, e^{j\frac{2\pi d}{\lambda}(M-1)\sin\theta_0}]^T$, $\mathbf{h}_{tr} = h_{tr}[1, e^{j\frac{2\pi d}{\lambda}\sin\theta_1}, \cdots, e^{j\frac{2\pi d}{\lambda}(M-1)\sin\theta_1}]^T$, and $\mathbf{w}(n)$ is CSCG noise vector distributed as $\mathbf{w}(n) \sim \mathcal{CN}(\mathbf{0}, \sigma^2\mathbf{I})$. Here, d is the distance between two adjacent antennas and λ is the wave length of the RF signal. Assume the delay distance at the mth antenna is $(m-1)d\sin\theta_i$ for $i \in \{0,1\}$ compared to the first antenna. Then it can be noticed that the equivalent channel at the mth antenna is

$$\begin{aligned}h_m &= h_{sr}e^{j\frac{2\pi d}{\lambda}(m-1)\sin\theta_0} + \eta h_{st}h_{tr}B(n)e^{j\frac{2\pi d}{\lambda}(m-1)\sin\theta_1}\\ &= h_0 e^{j\frac{2\pi d}{\lambda}(m-1)\sin\theta_0} + h_1 B(n)e^{j\frac{2\pi d}{\lambda}(m-1)\sin\theta_1},\end{aligned} \tag{2}$$

where $h_0 = h_{sr}$ and $h_1 = \eta h_{st}h_{tr}$.

Remark 1: Since h_m is a function of the modulated bit at the tag and channels h_{sr}, h_{st} and h_{tr}, it may be different from that in traditional point-to-point wireless communication systems. However, when the tag modulates bit '0', the effective channel reduces to the traditional communication channel.

[1]The channel h_{sr} is the traditional source to reader channel.

III. DoAs and Channel Gains Estimation

This section describes the procedure for the estimation of the DoAs and the channel gains. The technique is divided into the following three steps: i) the channel $\mathbf{h}$ in the absorptive or reflective state is incipiently retrieved by means of LS; ii) by performing DFT operation on the channel $\mathbf{h}$, coarse DoAs $[\theta_0, \theta_1]$ and gains $[h_0, \frac{h_1}{\eta}]$ can be obtained; and iii) with the aid of angular rotation, fine estimates of both the DoAs and the channel gains are acquired.

Step 1: Initial Channel Estimation

Prior to the tag modulates its own data, while the tag initially transmits $2N$ control sequences, the RF source transmits $2N$ pilots. Specifically, the tag transmits bit '0' during the first N RF symbols and bit '1' during the following N RF symbols. For $B(n) = i, i \in \{0,1\}$, we denote N RF pilots as $\mathbf{s} = [s_1, s_2, \cdots, s_N]^T$ and each element has modulus $\sqrt{P_s}$, i.e., $|\mathbf{s}_n|^2 = P_s$. Then, the received signal matrix of size $M \times N$ at the reader is

$$\mathbf{Y} = \mathbf{h}\mathbf{s}^T + \mathbf{W}, \tag{3}$$

where $\mathbf{W}$ is the $M \times N$ noise matrix. Then, an LS estimator for the desired channel $\mathbf{h}$ is

$$\hat{\mathbf{h}}^{\text{LS}} = \mathbf{Y}\mathbf{s}(\mathbf{s}^T\mathbf{s})^{-1} = \mathbf{h} + \frac{\mathbf{W}\mathbf{s}}{NP_s}. \tag{4}$$

Step 2: Coarse DoAs and Gains Estimation via DFT

We define the DFT matrix as

$$[\mathbf{F}]_{pq} = M^{-1}e^{-j\frac{2\pi}{M}(p-1)(q-1)}, \quad p,q \in \{1, \cdots, M\}. \tag{5}$$

Then, the DFT of the channel $\mathbf{h}$ is

$$\hat{\mathbf{h}}^{\text{DFT}} = \mathbf{F}\mathbf{h}, \tag{6}$$

whose mth entry can be calculated as

$$\begin{aligned}\hat{\mathbf{h}}_m^{\text{DFT}} &= \sum_{q=1}^{M}\frac{1}{M}e^{-j\frac{2\pi}{M}(m-1)(q-1)}\Big(h_0 e^{j\frac{2\pi d}{\lambda}(q-1)\sin\theta_0}\\ &\qquad + h_1 B(n)e^{j\frac{2\pi d}{\lambda}(q-1)\sin\theta_1}\Big)\\ &\overset{(a)}{=} \frac{h_0}{M}e^{-j\frac{M-1}{2}r_0}\frac{\sin(\frac{M}{2}r_0)}{\sin(\frac{1}{2}r_0)}\\ &\quad + \frac{h_1 B(n)}{M}e^{-j\frac{M-1}{2}r_1}\frac{\sin(\frac{M}{2}r_1)}{\sin(\frac{1}{2}r_1)},\end{aligned} \tag{7}$$

where (a) follows by using the formula of summation for geometric sequence, and $r_i = \frac{2\pi(m-1)}{M} - \frac{2\pi d}{\lambda}\sin\theta_i$ for $i \in \{0,1\}$. According to (7), if $\frac{Md}{\lambda}\sin\theta_i + 1$ is equal to certain integer m, $\hat{\mathbf{h}}^{\text{DFT}}$ has only one non-zero item $\hat{\mathbf{h}}_m^{\text{DFT}} = h_i$ when $M \to \infty$. This means that the channel power is centred on only one position $m = \frac{Md}{\lambda}\sin\theta_i + 1$. Further, the DoAs and the channel gains can be separately estimated as

$$\hat{\theta}_i^{\text{DFT}} = \begin{cases}\arcsin\left(\frac{(m-1-M)\lambda}{Md}\right), & \theta_i \in [-\frac{\pi}{2}, 0]\\ \arcsin\left(\frac{(m-1)\lambda}{Md}\right), & \theta_i \in [0, \frac{\pi}{2}]\end{cases} \tag{8}$$

$$\hat{h}_i^{\text{DFT}} = \hat{\mathbf{h}}_m^{\text{DFT}}. \tag{9}$$

However, the actual situation is that $\frac{Md}{\lambda}\sin\theta_i$ is not always an integer, where we can take $m = \lfloor\frac{Md}{\lambda}\sin\theta_0\rceil + 1$.

Step 3: Refining Estimates Through Angular Rotation Performing angular rotation operation yields

$$\hat{\mathbf{h}}^{\mathrm{Ro}} = \mathbf{F}\mathbf{\Phi}(\Delta_i)\mathbf{h}, \tag{10}$$

where $\mathbf{\Phi}(\Delta_i) = \mathrm{diag}\{1, e^{j\Delta_i}, \cdots, e^{j(M-1)\Delta_i}\}$ is angular rotation matrix for $\Delta_i \in [-\frac{\pi}{M}, \frac{\pi}{M}]$. Similarly, the mth element of $\hat{\mathbf{h}}^{\mathrm{Ro}}$ has the form as

$$\begin{aligned}\hat{\mathbf{h}}^{\mathrm{Ro}}_m =& \frac{h_0}{\sqrt{M}} e^{-j\frac{M-1}{2}\tilde{r}_0} \frac{\sin(\frac{M}{2}\tilde{r}_0)}{\sin(\frac{1}{2}\tilde{r}_0)} \\ &+ \frac{h_1 B(n)}{\sqrt{M}} e^{-j\frac{M-1}{2}\tilde{r}_1} \frac{\sin(\frac{M}{2}\tilde{r}_1)}{\sin(\frac{1}{2}\tilde{r}_1)},\end{aligned} \tag{11}$$

where $\tilde{r}_i = \frac{2\pi(m-1)}{M} - \frac{2\pi d}{\lambda}\sin\theta_i - \Delta_i$ for $i \in \{0, 1\}$. Obviously, there always exists Δ_i which makes

$$m = \frac{Md}{\lambda}\sin\theta_i + \frac{M\Delta_i}{2\pi} + 1, \tag{12}$$

an integer. Then, we can refine the corresponding parameters as

$$\hat{\theta}_i^{\mathrm{Ro}} = \begin{cases} \arcsin\left(\frac{(m-1-M)\lambda}{Md} - \frac{\Delta_i\lambda}{2\pi d}\right), & \theta_i \in [-\frac{\pi}{2}, 0] \\ \arcsin\left(\frac{(m-1)\lambda}{Md} - \frac{\Delta_i\lambda}{2\pi d}\right), & \theta_i \in [0, \frac{\pi}{2}] \end{cases} \tag{13}$$

$$\hat{h}_i^{\mathrm{Ro}} = \hat{\mathbf{h}}_m^{\mathrm{Ro}}. \tag{14}$$

Remark 2: The presented method is also applicable to channel estimation in multi-path or frequency-selective channels scenarios since the composite channel in the case of $B(n) = 1$ can be treated as a combination of paths $S-R$ and $S-T-R$.

IV. Cramér-Rao Lower Bounds

In this section, we compute the CRLBs for the modulus of the channel gain and the DoA estimates. Suppose $h_0 = |h_0|e^{j\omega_0}$ and $h_1 = |h_1|e^{j\omega_1}$. Let us define vector $\boldsymbol{\varphi} = [|h_0|, |h_1|, \sin\theta_0, \sin\theta_1]^T$ and $g(\boldsymbol{\varphi}) = [|h_0|, \frac{|h_1|}{\eta}, \theta_0, \theta_1]^T$. For a given $\boldsymbol{\varphi}$, the probability density function $p(\mathbf{y}; \boldsymbol{\varphi})$ of $\mathbf{y} = [\mathbf{y}^T(N+1), \cdots, \mathbf{y}^T(2N)]^T$ during N consecutive RF signals is

$$p(\mathbf{y}; \boldsymbol{\varphi}) = \frac{\pi^{-MN}}{\sigma^{2MN}} \prod_{n=N+1}^{2N} e^{-\frac{\|\mathbf{y}(n) - (\mathbf{h}_{sr} + \eta h_{st}\mathbf{h}_{tr})s(n)\|^2}{\sigma^2}}. \tag{15}$$

The Fisher information matrix of vector $\boldsymbol{\varphi}$ is defined as [20]

$$[\mathbf{I}(\boldsymbol{\varphi})]_{m,n} = -\mathbb{E}\left\{\frac{\partial^2 \ln p(\mathbf{y}; \boldsymbol{\varphi})}{\partial\boldsymbol{\varphi}_m \partial\boldsymbol{\varphi}_n}\right\}. \tag{16}$$

Let $c_0 = \frac{2\pi d}{\lambda}$, $c_1 = \frac{2\pi d}{\lambda}(\sin\theta_0 - \sin\theta_1)$ and $c_2 = \omega_0 - \omega_1$, and the Fisher information matrix and its entries are

$$\mathbf{I}(\boldsymbol{\varphi}) = \frac{2\sum_{n=N+1}^{2N}|s(n)|^2}{\sigma^2} \begin{pmatrix} T_{11} & T_{12} & 0 & T_{14} \\ T_{12} & T_{22} & T_{23} & 0 \\ 0 & T_{23} & T_{33} & T_{34} \\ T_{14} & 0 & T_{34} & T_{44} \end{pmatrix}, \tag{17}$$

$$\begin{aligned} T_{11} &= M,\ T_{12} = \sum_{m=0}^{M-1}\cos(c_1 m + c_2), \\ T_{14} &= c_0|h_1|\sum_{m=0}^{M-1} m\sin(c_1 m + c_2),\ T_{22} = M, \\ T_{23} &= -c_0|h_0|\sum_{m=0}^{M-1} m\sin(c_1 m + c_2), \\ T_{33} &= c_0^2 h_0^2 (M-1)M(2M-1)/6, \\ T_{34} &= c_0^2|h_0 h_1|\sum_{m=0}^{M-1} m^2\cos(c_1 m + c_2), \\ T_{34} &= c_0^2|h_0 h_1|\sum_{m=0}^{M-1} m^2\cos(c_1 m + c_2), \\ T_{44} &= c_0^2 h_1^2 (M-1)M(2M-1)/6. \end{aligned}$$

The proof of (17) is given in Appendix.

Afterwards, the CRLB of the estimate $\hat{g}(\boldsymbol{\varphi})$ of $g(\boldsymbol{\varphi})$ can be derived by using the equality:

$$\begin{aligned}\mathrm{CRLB}\Big([\hat{g}(\boldsymbol{\varphi})]_{m,1}\Big) &= \left[\frac{\partial g(\boldsymbol{\varphi})}{\partial\boldsymbol{\varphi}}\mathbf{I}^{-1}(\boldsymbol{\varphi})\frac{\partial g(\boldsymbol{\varphi})}{\partial\boldsymbol{\varphi}}^T\right]_{mm} \\ &= \left[\frac{\partial g(\boldsymbol{\varphi})}{\partial\boldsymbol{\varphi}}\right]_{mm}^2 [\mathbf{I}^{-1}(\boldsymbol{\varphi})]_{mm},\end{aligned} \tag{18}$$

where $\frac{\partial g(\boldsymbol{\varphi})}{\partial\boldsymbol{\varphi}} = \mathrm{diag}\left\{1, \frac{1}{\eta}, \frac{1}{\cos\theta_0}, \frac{1}{\cos\theta_1}\right\}$.

Based on (17) and (18), the CRLBs of the modulus of the channel gains and the DoAs estimates in the case of $B(n) = 1$ can be respectively formulated as

$$\begin{aligned}\mathrm{CRLB}\left(|\hat{h}_0|\right) &= \frac{\sigma^2(T_{22}T_{33}T_{44} - T_{22}T_{34}^2 - T_{23}^2T_{44})}{2L_1\sum_{n=N+1}^{2N}|s(n)|^2}, \\ \mathrm{CRLB}\left(\frac{|\hat{h}_1|}{\eta}\right) &= \frac{\sigma^2(T_{11}T_{33}T_{44} - T_{14}^2T_{33} - T_{11}T_{34}^2)}{2L_1\eta^2\sum_{n=N+1}^{2N}|s(n)|^2}, \\ \mathrm{CRLB}\left(\hat{\theta}_0\right) &= \frac{\sigma^2(T_{11}T_{22}T_{44} - T_{22}T_{14}^2 - T_{12}^2T_{44})}{2L_1\cos^2\theta_0\sum_{n=N+1}^{2N}|s(n)|^2}, \\ \mathrm{CRLB}\left(\hat{\theta}_1\right) &= \frac{\sigma^2(T_{11}T_{22}T_{33} - T_{11}T_{23}^2 - T_{12}^2T_{33})}{2L_1\cos^2\theta_1\sum_{n=N+1}^{2N}|s(n)|^2},\end{aligned} \tag{19}$$

where

$$\begin{aligned}L_1 =& \Big(T_{14}^2(T_{23}^2 - T_{22}T_{33}) - 2T_{12}T_{14}T_{23}T_{34} \\ &+ (T_{12}^2 - T_{11}T_{22})(T_{34}^2 - T_{33}T_{44}) - T_{11}T_{23}^2T_{44}\Big).\end{aligned}$$

Considering that $[\mathbf{I}^{-1}(\boldsymbol{\varphi})]_{mm} \geq [\mathbf{I}(\boldsymbol{\varphi})]_{mm}^{-1}$, we obtain a lower bound of CRLBs (LCRLBs) in the case of $B(n) = 1$ as

$$\mathrm{LCRLB}\Big([\hat{g}(\boldsymbol{\varphi})]_{m,1}\Big) = \left[\frac{\partial g(\boldsymbol{\varphi})}{\partial\boldsymbol{\varphi}}\right]_{mm}^2 \frac{1}{[\mathbf{I}(\boldsymbol{\varphi})]_{mm}}. \tag{20}$$

Consequently, the corresponding LCRLBs can be shown as

$$\mathrm{LCRLB}\left(|\hat{h}_0|\right) = \frac{(2M)^{-1}\sigma^2}{\sum_{n=N+1}^{2N}|s(n)|^2}, \tag{21}$$

$$\mathrm{LCRLB}\left(\frac{|\hat{h}_1|}{\eta}\right) = \frac{(2M\eta^2)^{-1}\sigma^2}{\sum_{n=N+1}^{2N}|s(n)|^2}, \tag{22}$$

$$\mathrm{LCRLB}\left(\hat{\theta}_0\right) = \frac{3M^{-1}(2\pi dh_0\cos\theta_0)^{-2}\lambda^2\sigma^2}{(M-1)(2M-1)\sum_{n=N+1}^{2N}|s(n)|^2}, \tag{23}$$

$$\mathrm{LCRLB}\left(\hat{\theta}_1\right) = \frac{3M^{-1}(2\pi dh_1\cos\theta_1)^{-2}\lambda^2\sigma^2}{(M-1)(2M-1)\sum_{n=N+1}^{2N}|s(n)|^2}. \tag{24}$$

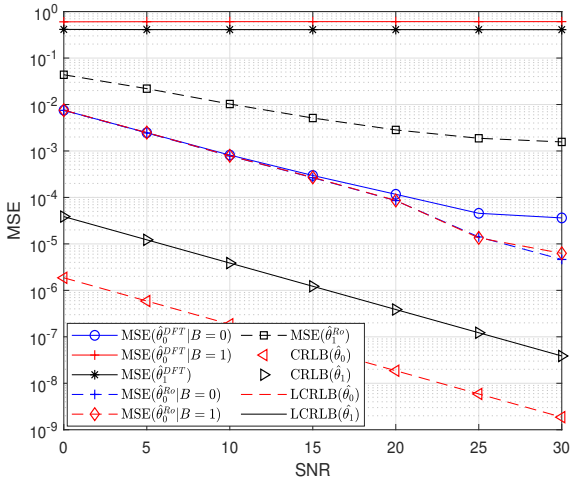

Fig. 2. MSE of DoA versus transmit SNR.

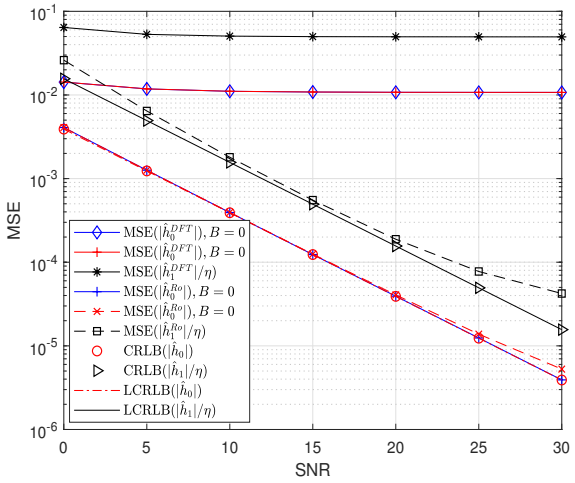

Fig. 3. MSE of the modulus of channel gain versus transmit SNR.

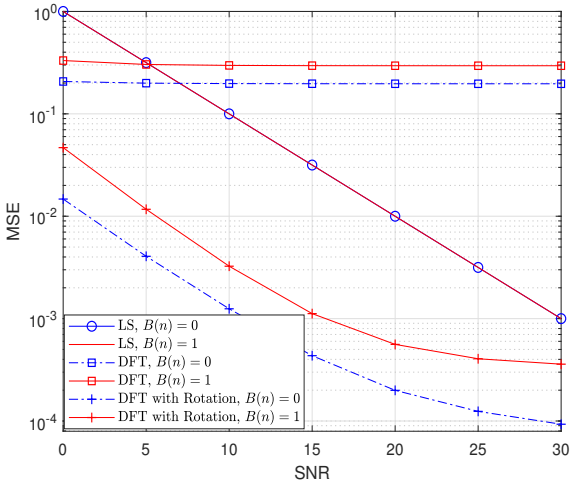

Fig. 4. MSE of channel versus transmit SNR.

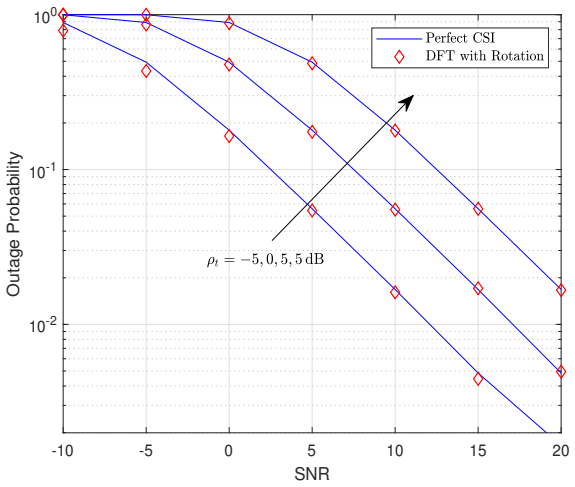

Fig. 5. Outage probability versus transmit SNR.

In a similar way, the CRLBs of the modulus of the channel gain and the DoA estimates for $B(n) = 0$ can be derived as (21) and (23) just by replacing the range of n with $\{1, \cdots, N\}$, respectively.

Remark 3: As shown in Fig. 2 and Fig. 3, the related curves of the CRLBs and LCRLBs fit well. Accordingly, we can replace the CRLBs (19) with LCRLBs (21)-(24), which are more straightforward for performance analysis.

V. Simulation Results

In this section, we select $N = 1$, $\sigma^2 = 1$ and $\eta = 0.5$. The reader is configured with $M = 128$ antennas. The DoAs are set to $\theta_0 = -\frac{\pi}{4}$ and $\theta_1 = \frac{\pi}{5}$. All fading channels are modeled as $h_0, h_{st}, h_{tr} \sim \mathcal{CN}(0, 1)$. Here, the mean square error (MSE) of an estimator $\hat{x}$ is the average squared difference between the estimated result $\hat{x}$ and what is estimated x, i.e., $\mathrm{MSE}(\hat{x}) = \mathbb{E}\{(x - \hat{x})^2\}$.

Fig. 2 displays MSEs of DoAs versus transmit SNR and Fig. 3 shows MSEs of the modulus of channel gains versus transmit SNR. According to our analysis in Section IV, the CRLBs of the estimates $\hat{\theta}_0$ and $|\hat{h}_0|$ of θ_0 and $|h_0|$ in the case of $B(n) = 0$ are equal to the corresponding LCRLBs in the case of $B(n) = 1$. Therefore, we omit the CRLB curves in the case of $B(n) = 0$. Both MSEs and CRLBs of the DoAs and the modulus of channel gains estimates decrease with the increase of transmit SNR. It can be found that the corresponding CRLB curves are exactly below the corresponding MSE curves of our proposed estimator, which verifies the validity of our theoretical derivations in (19).

Fig. 4 depicts MSEs of estimates of $\mathbf{h}$ versus transmit signal-to-noise ratio (SNR). As expected, the DFT-based estimator with angular rotation ('+' marked curves) performs better than that without rotation ('□' marked curves). We also observe that DFT-based estimator with angular rotation outperforms the traditional LS estimator (solid curves).

To show the impact of our proposed channel estimation on actual performance, Fig. 5 illustrates outage probability versus transmit SNR when threshold ρ_t is set to $-5, 0, 5$ dB, where we use the selection combining reception at the reader. It can be seen that the gap between outage performance with perfect CSI assumption and that with channel estimated by our proposed method is negligible over the simulated range.

VI. Conclusion

In this paper, we propose a channel estimation technique for an ambient backscatter communication system with a massive-antenna reader. We tackle the channel estimation problem based on a signal processing standpoint as channels can be decomposed into channel gains and DoAs. First, preliminary channel estimations at different states are acquired by the LS estimation. Coupled with angular rotation, we then obtain both the channel gains and the DoAs by conducting DFT to the estimates. It is revealed that the proposed method separately features high estimation accuracy and low complexity compared to the LS and EVD estimators.

Appendix

Suppose $s(n) = |s(n)|e^{j\omega_{s_n}}$, then taking the log-likelihood function of $p(\mathbf{y};\boldsymbol{\varphi})$ (15) produces

$$\ln p(\mathbf{y};\boldsymbol{\varphi}) = -MN\ln(\pi\sigma^2) - \frac{1}{\sigma^2}\sum_{n=N+1}^{2N}\sum_{m=1}^{M} \tag{25}$$
$$\Big[\big(\mathfrak{Re}\{\mathbf{y}_m(n)\} - |s(n)|\sum_{i=1}^{2}\boldsymbol{\varphi}_i\cos(c_0m\boldsymbol{\varphi}_{i+2}+\omega_i+\omega_{s_n})\big)^2 +$$
$$\big(\mathfrak{Im}\{\mathbf{y}_m(n)\} - |s(n)|\sum_{i=1}^{2}\boldsymbol{\varphi}_i\sin(c_0m\boldsymbol{\varphi}_{i+2}+\omega_i+\omega_{s_n})\big)^2\Big],$$

where $\mathbb{E}\{\mathfrak{Re}\{\mathbf{y}_m(n)\}\} = |s(n)|\sum_{i=1}^{2}\boldsymbol{\varphi}_i\cos(c_0m\boldsymbol{\varphi}_{i+2}+\omega_i+\omega_{s_n})$ and $\mathbb{E}\{\mathfrak{Im}\{\mathbf{y}_m(n)\}\} = |s(n)|\sum_{i=1}^{2}\boldsymbol{\varphi}_i\sin(c_0m\boldsymbol{\varphi}_{i+2}+\omega_i+\omega_{s_n})$.

For $i \neq j, i, j \in \{1,2\}$, taking the negative second derivatives of (25) yield

$$-\frac{\partial^2\ln p(\mathbf{y};\boldsymbol{\varphi})}{\partial\boldsymbol{\varphi}_i^2} = \frac{2M}{\sigma^2}\sum_{n=N+1}^{2N}|s(n)|^2,$$

$$-\frac{\partial^2\ln p(\mathbf{y};\boldsymbol{\varphi})}{\partial\boldsymbol{\varphi}_i\partial\boldsymbol{\varphi}_j} = \frac{2}{\sigma^2}\sum_{n=N+1}^{2N}|s(n)|^2\sum_{m=1}^{M}\cos(c_1m+c_2),$$

$$-\frac{\partial^2\ln p(\mathbf{y};\boldsymbol{\varphi})}{\partial\boldsymbol{\varphi}_i\partial\boldsymbol{\varphi}_{i+2}} = \sum_{n=N+1}^{2N}\frac{2|s(n)|}{\sigma^2}\sum_{m=1}^{M}\Big(|s(n)|\boldsymbol{\varphi}_j c_0 m\times$$
$$\sin(c_1m+c_2) + \mathfrak{Re}\{\mathbf{y}_m(n)\}c_0m\sin(c_0m\boldsymbol{\varphi}_{i+2}+\omega_i+\omega_{s_n})$$
$$-\mathfrak{Im}\{\mathbf{y}_m(n)\}c_0m\cos(c_0m\boldsymbol{\varphi}_{i+2}+\omega_i+\omega_{s_n})\Big),$$

$$-\frac{\partial^2\ln p(\mathbf{y};\boldsymbol{\varphi})}{\partial\boldsymbol{\varphi}_i\partial\boldsymbol{\varphi}_{j+2}} = \sum_{n=N+1}^{2N}\frac{2|s(n)|^2}{\sigma^2}\sum_{m=1}^{M}\Big(\boldsymbol{\varphi}_j c_0 m\times$$
$$\sin\big(c_0m(\boldsymbol{\varphi}_{i+2}-\boldsymbol{\varphi}_{j+2})+\omega_i-\omega_j\big)\Big),$$

$$-\frac{\partial^2\ln p(\mathbf{y};\boldsymbol{\varphi})}{\partial\boldsymbol{\varphi}_{i+2}^2} = \sum_{n=N+1}^{2N}\frac{2|s(n)|}{\sigma^2}\sum_{m=1}^{M}\Big(-|s(n)|\boldsymbol{\varphi}_i\boldsymbol{\varphi}_j c_0^2m^2$$
$$\times\cos(c_1m+c_2) + \mathfrak{Re}\{\mathbf{y}_m(n)\}\boldsymbol{\varphi}_i c_0^2m^2\cos(c_0m\boldsymbol{\varphi}_{i+2}+\omega_i$$
$$+\omega_{s_n}) + \mathfrak{Im}\{\mathbf{y}_m(n)\}\boldsymbol{\varphi}_i c_0^2m^2\sin(c_0m\boldsymbol{\varphi}_{i+2}+\omega_i+\omega_{s_n})\Big),$$

$$-\frac{\partial^2\ln p(\mathbf{y};\boldsymbol{\varphi})}{\partial\boldsymbol{\varphi}_{i+2}\partial\boldsymbol{\varphi}_{j+2}} = \boldsymbol{\varphi}_i\boldsymbol{\varphi}_j\sum_{n=N+1}^{2N}\frac{2c_0^2|s(n)|^2}{\sigma^2}\times$$
$$\sum_{m=1}^{M}m^2\cos(c_1m+c_2).$$

Upon averaging the derivatives with respect to $\mathfrak{Re}\{\mathbf{y}_m(n)\}$ and $\mathfrak{Im}\{\mathbf{y}_m(n)\}$, we have entries as shown in (17).

References

[1] Y. Zhou, H. Liu, Z. Pan, L. Tian, and J. Shi, "Spectral- and energy-efficient two-stage cooperative multicast for LTE-Advanced and beyond," *IEEE Wireless Commun. Mag.*, vol. 21, no. 2, pp. 34–41, Apr. 2014.

[2] A. Al-Fuqaha, M. Guizani, M. Mohammadi, M. Aledhari, and M. Ayyash, "Internet of Things: A survey on enabling technologies, protocols, and applications," *IEEE Commun. Surveys Tuts.*, vol. 17, no. 4, pp. 2347–2376, Jun. 2015.

[3] V. Liu, A. Parks, V. Talla, S. Gollakota, D. Wetherall, and J. R. Smith, "Ambient backscatter: wireless communication out of thin air," in *Proc. SIGCOMM*, Hong Kong, China, Aug. 2013, pp. 39–50.

[4] Q. Tao, C. Zhong, K. Huang, X. Chen, and Z. Zhang, "Ambient backscatter communication systems with MFSK modulation," *IEEE Trans. Wireless Commun.*, vol. 18, no. 5, pp. 2553–2564, May 2019.

[5] Q. Tao, C. Zhong, H. Lin, and Z. Zhang, "Symbol detection of ambient backscatter systems with Manchester coding," *IEEE Trans. Wireless Commun.*, vol. 17, no. 6, pp. 4028–4038, Jun. 2018.

[6] W. Zhao, G. Wang, R. Fan, L. S. Fan, and S. Atapattu, "Ambient backscatter communication systems: Capacity and outage performance analysis," *IEEE Access*, vol. 6, no. 1, pp. 22 695–22 704, 2018.

[7] W. Zhao, G. Wang, S. Atapattu, C. Tellambura, and H. Guan, "Outage analysis of ambient backscatter communication systems," *IEEE Commun. Lett.*, vol. 22, no. 8, pp. 1736–1739, Aug. 2018.

[8] D. Li and Y. Liang, "Adaptive ambient backscatter communication systems with MRC," *IEEE Trans. Veh. Technol.*, vol. 67, no. 12, pp. 12 352–12 357, Dec. 2018.

[9] W. Liu, Y. Liang, Y. Li, and B. Vucetic, "Backscatter multiplicative multiple-access systems: Fundamental limits and practical design," *IEEE Trans. Wireless Commun.*, vol. 17, no. 9, pp. 5713–5728, Sep. 2018.

[10] Y. Zou, J. Zhu, X. Li, and L. Hanzo, "Relay selection for wireless communications against eavesdropping: a security-reliability trade-off perspective," *IEEE Network*, vol. 30, no. 5, pp. 74–79, Sep. 2016.

[11] J. Zhu, Y. Zou, B. Champagne, W. Zhu, and L. Hanzo, "Security-reliability tradeoff analysis of multirelay-aided decode-and-forward cooperation systems," *IEEE Trans. Veh. Technol.*, vol. 65, no. 7, pp. 5825–5831, Jul. 2016.

[12] J. Zhu and Y. Zou, "Cognitive network cooperation for green cellular networks," *IEEE Access*, vol. 4, pp. 849–857, 2016.

[13] S. Ma, G. Wang, R. Fan, and C. Tellambura, "Blind channel estimation for ambient backscatter communication systems," *IEEE Commun. Lett.*, vol. 22, no. 6, pp. 1296–1299, Jun. 2018.

[14] W. Zhao, G. Wang, S. Atapattu, and B. Ai, "Blind channel estimation in ambient backscatter communication systems with multiple-antenna reader," in *IEEE/CIC Int. Conf. Commun. in China (ICCC)*, Beijing, China, Aug. 2018, pp. 320–324.

[15] J. Ma, S. Zhang, H. Li, N. Zhao, and V. C. M. Leung, "Interference-alignment and soft-space-reuse based cooperative transmission for multi-cell massive MIMO networks," *IEEE Trans. Wireless Commun.*, vol. 17, no. 3, pp. 1907–1922, Mar. 2018.

[16] S. Atapattu, N. Ross, Y. Jing, Y. He, and J. S. Evans, "Physical-layer security in full-duplex multi-hop multi-user wireless network with relay selection," *IEEE Trans. Wireless Commun.*, vol. 18, no. 2, pp. 1216–1232, Feb. 2019.

[17] B. Wang, F. Gao, S. Jin, H. Lin, and G. Y. Li, "Spatial- and frequency-wideband effects in millimeter-wave massive MIMO systems," *IEEE Trans. Signal Processing*, vol. 66, no. 13, pp. 3393–3406, Jul. 2018.

[18] D. Fan, F. Gao, G. Wang, Z. Zhong, and A. Nallanathan, "Angle domain signal processing-aided channel estimation for indoor 60-GHz TDD/FDD massive MIMO systems," *IEEE J. Select. Areas Commun.*, vol. 35, no. 9, pp. 1948–1961, Sep. 2017.

[19] G. Wang, F. Gao, R. Fan, and C. Tellambura, "Ambient backscatter communication systems: Detection and performance analysis," *IEEE Trans. Commun.*, vol. 64, no. 11, pp. 4836–4846, Nov. 2016.

[20] C. W. Helstrom, *Elements of signal detection and estimation*. Prentice-Hall, Inc., 1994.